46th AIAA/ASME/SAE/ASEE Joint Propulsion Conference & Exhibit
25 - 28 July 2010, Nashville, TN

AIAA 2010-6801

Axially Traveling Waves in Porous Tubes with Arbitrary Crossflow Velocity

Todd A. Jankowski* and Joseph Majdalani†
University of Tennessee Space Institute, Tullahoma, TN 37388

This paper devotes itself to the development of an asymptotic representation of the axially traveling wave in porous tubes with arbitrary levels of wall suction or injection. The analysis starts by splitting the viscous Navier-Stokes equations into both a steady and a time-dependent part. The steady part can be solved using Berman's similarity solution, thus giving rise to a Hart-McClure or Taylor-Culick type models. The unsteady part is decomposed using the Helmholtz vector theorem into a compressible irrotational component and a solenoidal rotational part. Each set is solved separately and then coupled through the wall boundary condition. The ensuing rotational field consists of a doubly-perturbed problem that can be treated using multiple-scales and WKB techniques. The perturbations are carried out in the reciprocal of the crossflow Reynolds number *R*, while assuming a Strouhal number of the same order as *R*. At the outset, a general WKB formulation for the wave motion is obtained from which the cases of wall injection or suction may be readily extracted. The character of the solution is found to be consistent with that of a weakly under-damped wave that is strongly influenced by the mean flow profile prescribed in the chamber. A multiple-scales expansion is also undertaken, thus helping to unravel the inner scaling structure associated with this problem. Our approach applies to the case of suction where a linear scaling constitution is established. For the case of wall injection, a nonlinear scaling transformation will be required and this will be demonstrated in a forthcoming study where a generalized-scaling technique will be employed. By way of verification, two closed-form multiple-scales and WKB expressions are retrieved for the case of large crossflow Reynolds number and shown to compare quite favorably with an exact limiting process solution. Finally, the Stokes layer thickness and Richardson annular effect associated with this model are briefly captured and discussed.

Nomenclature

A	= dimensional pressure wave amplitude
a	= tube radius
$a(\eta)$	= coefficient in the generalized separated momentum equation
$a_0(\eta)$	= leading-order term in $a(\eta)$
$a_1(\eta)$	= higher order term in $a(\eta)$
A_1	= integration function from the multiple-scales analysis
A_2	= integration function from the multiple-scales analysis
a_s	= stagnation speed of sound
$b(\eta)$	= coefficient in the generalized separated momentum equation
$b_0(\eta)$	= leading-order term in $b(\eta)$
$b_1(\eta)$	= first order term in $b(\eta)$
$c(\eta)$	= coefficient in the generalized separated momentum equation
E_n	= maximum absolute error between an asymptotic solution and the exact solution

*Research Associate and Former Graduate Student. Presently: Research and Development Engineer, Mechanical and Thermal Engineering Group, Los Alamos National Laboratory.
†H. H. Arnold Chair of Excellence in Advanced Propulsion, Mechanical, Aerospace and Biomedical Engineering Department. Senior Member AIAA. Fellow ASME.

F = mean flow similarity parameter
F_0 = the mean flow similarity parameter, F, evaluated at the wall
G = dependent variable used in the generalized separated momentum equation
i = $(-1)^{1/2}$
L = dimensional tube length
l = nondimensional tube length
L_c = characteristic length dimension
M = Mach number
m = oscillation mode number
p = pressure
Q_j = functional argument of the WKB expansion
R = crossflow Reynolds number
r = radial coordinate
S = Strouhal number
t = time
$\boldsymbol{u}$ = velocity vector
U_w = wall velocity
$X(x)$ = r-independent velocity function
x = axial coordinate
$Y_n(r)$ = x-independent velocity function
z = stretched coordinate near the wall or a dummy variable used for integration

ε = the inverse of the crossflow Reynolds number
$\bar{\varepsilon}$ = nondimensional pressure wave amplitude
Φ = confluent hypergeometric function
γ = the ratio of specific heats
η = independent variable used in the generalized separated momentum equation
κ_n = momentum equation separation eigenvalue
μ^* = fluid dynamic viscosity
ν = fluid kinematic viscosity
ρ = density
τ^* = shear stress tensor
ω = nondimensional circular frequency
ω_s = dimensional circular frequency
χ = stretched length scale near the porous wall
Ψ = steady stream function
∇ = nondimensional del operator

Subscripts
0,1,… = the order of approximation in a perturbation series
s = stagnation value of a quantity

Superscripts
* = dimensional quantity
^ = acoustic component
~ = vortical component

I. Introduction

SINCE Berman's landmark paper,[1] extensive studies into the problem of flows in porous tubes and channels with wall suction or injection have been undertaken. These proved essential to a variety of technological applications including membrane separation processes,[1,2] transpiration cooling,[3] jet mixing,[4,5] boundary layer control,[6-9] and propellant burning.[10-16] In modeling the flowfield inside solid rocket motors, Berman-based solutions have formed the backbone of most mean flow models used to describe the bulk gaseous motion. These include the Hart-

McClure,[17,18] Taylor,[19-21] and Taylor-Culick[22] steady-state profiles under both incompressible and compressible flow conditions.[23,24] In recent work, Berman's similarity-based equation has given rise to several innovative mathematical solutions based on quasi-linearization,[25] Lie-group theory,[26,27] the Adomian decomposition method,[28] the homotopy-perturbation method (HPM),[29] and the homotopy-analysis method (HAM).[30,31] The latter was shown to provide series approximations that remained independent of the size of the crossflow Reynolds number.[31]

Berman first studied the porous channel flow by reducing the Navier-Stokes equations to a single, fourth order, non-linear ordinary differential equation (ODE) through the use of a steady stream function. Berman then solved this ODE via regular perturbations, with the crossflow Reynolds number as a small parameter. Berman's crossflow Reynolds number is traditionally written as $R = U_w L_c / \nu$, thus combining the wall suction velocity U_w and a characteristic dimension L_c. For the rectangular channel, L_c is taken to be the channel half-height h, while for the porous tube, the radius a is substituted. In the case of wall injection, one simply replaces the velocity by $-U_w$.

By taking R as the perturbation parameter, Berman managed to obtain solutions that could be used for small Reynolds number. Based on Berman's equation, numerous studies emerged and these were concerned with the need to generate accurate descriptions of the steady flow in both channels and tubes undergoing different levels of suction or injection. In this vein, Yuan[32,33] extended Berman's range, in both channel and tube geometries, to $R = 20$, while Sellars[34] and Terrill[35] developed exact solutions as $R \to \infty$.

Naturally, these past studies have been focused on the non-oscillatory motion developed due to suction or injection at the boundaries. However, random fluctuations in the crossflow velocity are often inevitable and take place over a wide spectrum of frequencies. Those matching the enclosure's natural modes can give rise to a self-sustaining acoustic field that exhibits rich fluid dynamical structures.[36-38] Additionally, the modeling of the respiratory and circulatory functions of the body exhibit an externally induced oscillatory field that is of interest to physiologists.[39] Although the problem of oscillatory flows in tubes and channels without suction or injection at the walls has been extensively studied in the past,[40-42] and despite the availability of models to describe the oscillatory flow in porous tubes with arbitrary levels of wall injection,[43,44] no solutions have been developed to model the oscillatory flow in porous tubes with *arbitrary* levels of suction.

In this article, we present mathematical generalizations to describe the oscillatory velocity field in a porous tube that is subjected to arbitrary levels of wall suction. The solutions obtained here will apply equally well to the modeling of injection-driven oscillatory waves in porous enclosures, such as simulated rocket motors, although the converse may not always hold. An analytical formulation of the oscillatory velocity field in a porous tube may be viewed as a basic contribution to viscous boundary-layer theory. The technique to be used will rely on perturbation theory and the differential equation ultimately describing the time-dependent velocity for arbitrary suction will be solved using both multiple-scales and WKB expansion methods. In addition, an exact solution for the problem, which was derived under special suction conditions,[37] will be used to verify the asymptotic approximations. The particular equation to be examined with perturbation tools exemplifies the elements of analysis associated with a doubly-perturbed problem that needs to be solved for large Reynolds and Strouhal numbers. The procedure leading to its simplification into a singly-perturbed problem may be by itself a valuable maneuver in asymptotic analysis. The same approach may have applications in the treatment of similar differential equations that are encountered in modeling complex physical processes that entail co-existing dispersive and dissipative mechanisms.

II. Problem Formulation

A. Basic Flow Model

Our enclosure consists of a long slender tube with a porous wall and radius a. Although wall injection can be considered as in the simulation of solid rocket chambers,[43] we adopt the more general case of a fluid being withdrawn from the porous surface at a uniform wall velocity U_w. The length of the tube is defined as L, and symmetry about the longitudinal axis is assumed. This enables us to reduce the solution domain to $0 \le x \le l$, and $0 \le r \le 1$, where $l = L/a$ is the dimensionless tube length. To illustrate the cylindrical geometry, Fig. 1 is provided to present a cross-section of the tube with the mean flow streamlines calculated from Terrill's model for large suction.[35]

Under the influence of small variations in the crossflow velocity, a tube or channel that is rigid at the head end and isobarically open at the aft end can develop longitudinal pressure oscillations of amplitude A. The corresponding acoustic frequency is specified by

$$\omega_s = (m - \tfrac{1}{2})\pi a_s / L, \tag{1}$$

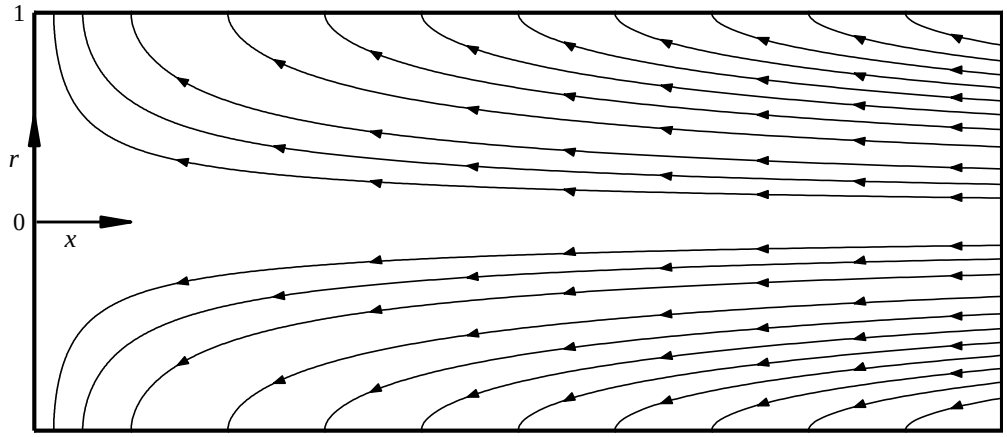

Figure 1. System geometry showing mean flow streamlines.

where a_s refers to the stagnation speed of sound, and m is the oscillation mode number.

In order to simplify the analysis to the point where an analytical solution can be attempted, several restrictions must be observed. First, the mean flow is assumed to be laminar. The mechanisms of mixing, swirling, or turbulence are also discounted. The fluid is restricted to Newtonian behavior, and the oscillatory pressure amplitude is taken to be small in comparison with the stagnation pressure.

B. Governing Equations

Employing asterisks to represent dimensional variables, density, pressure, time, velocity, and shear stress can be defined as ρ^*, p^*, t^*, $\boldsymbol{u}^*$, and τ^* respectively. Continuity and conservation of momentum are then presented in their general forms

$$\frac{\partial \rho^*}{\partial t^*} + \nabla^* \cdot \left(\rho^* \boldsymbol{u}^* \right) = 0 \tag{2}$$

$$\frac{\partial \left(\rho^* \boldsymbol{u}^* \right)}{\partial t^*} + \nabla^* \cdot \left(\rho^* \boldsymbol{u}^* \boldsymbol{u}^* \right) = -\nabla^* p^* - \left(\nabla^* \cdot \tau^* \right). \tag{3}$$

By using continuity to simplify the left-hand side of the equation of motion and by evaluating the viscous transfer term, Eq. (3) can be transformed into

$$\rho^* \left[\frac{\partial \boldsymbol{u}^*}{\partial t^*} + \left(\boldsymbol{u}^* \cdot \nabla^* \right) \boldsymbol{u}^* \right] = -\nabla^* p^* + \mu^* \left[\frac{4}{3} \nabla^* \left(\nabla^* \cdot \boldsymbol{u}^* \right) - \nabla^* \times \left(\nabla^* \times \boldsymbol{u}^* \right) \right], \tag{4}$$

where μ^* is the dynamic viscosity.

In order to generalize the analysis, dimensionless parameters are introduced. Spatial coordinates are normalized by a, the total instantaneous velocity by a_s, and time by the system's oscillation frequency ω_s. The normalized parameters are then defined as

$$x = x^*/a\,,\ r = r^*/a\,,\ t = \omega_s t^*,\ \boldsymbol{u} = \boldsymbol{u}^*/a_s\,,\ p = p^*/\gamma p_s \text{ and } \rho = \rho^*/\rho_s\,, \tag{5}$$

where ρ_s is the stagnation density, p_s is the stagnation pressure, and γ is the ratio of specific heats. Following this choice, Eqs. (2) and (4) become

$$\omega \frac{\partial \rho}{\partial t} + \nabla \cdot \left(\rho \boldsymbol{u} \right) = 0\,, \tag{6}$$

$$\rho \left[\omega \frac{\partial \boldsymbol{u}}{\partial t} + (\boldsymbol{u} \cdot \nabla) \boldsymbol{u} \right] = -\nabla p + M \varepsilon \left[4 \nabla \left(\nabla \cdot \boldsymbol{u} \right) / 3 - \nabla \times \left(\nabla \times \boldsymbol{u} \right) \right]. \tag{7}$$

The resulting set displays the non-dimensional frequency $\omega \equiv \omega_s a / a_s$, the suction Mach number $M \equiv U_w / a_s$, and the small parameter $\varepsilon \equiv 1/R$.

1. Perturbed Variables

With the introduction of small amplitude oscillations at a frequency ω_s, the instantaneous pressure can be expressed as the linear sum of the time-dependent and steady components:

$$p = p_0 + \bar{\varepsilon}\, p_1 \exp(-it)\,, \tag{8}$$

where $i = \sqrt{-1}$, $\bar{\varepsilon} = A/(\gamma p_s)$ is the pressure wave amplitude, and $\mathcal{O}(\varepsilon)$ and p_1 are only functions of space. Noting that the mean flow solutions have been developed for incompressible flow, the density can be expanded in a similar fashion by putting

$$\rho = 1 + \bar{\varepsilon}\rho_1 \exp(-it)\,. \tag{9}$$

Finally, the total velocity may be expressed as

$$\boldsymbol{u} = M\boldsymbol{u}_0 + \bar{\varepsilon}\,\boldsymbol{u}_1 \exp(-it)\,. \tag{10}$$

Note that the Mach number appears in the definition of the mean flow velocity because $\boldsymbol{u}_0$ represents the $\mathcal{O}(1)$ steady velocity normalized by U_w.

2. Leading-order Decomposition

Equations (8)–(10) must be inserted back into Eqs. (6)–(7). The zero-order terms yield the mean flow equations

$$\nabla\cdot\boldsymbol{u}_0 = 0 \tag{11}$$

$$M^2(\boldsymbol{u}_0\cdot\nabla)\boldsymbol{u}_0 = -\nabla p_0 + M^2\varepsilon\left[\tfrac{4}{3}\nabla(\nabla\cdot\boldsymbol{u}_0) - \nabla\times(\nabla\times\boldsymbol{u}_0)\right]. \tag{12}$$

A steady stream function that observes Berman's similarity form[1] may be written in terms of a characteristic mean flow function F where

$$\Psi = -xF(r)\,. \tag{13}$$

The velocity components can then be expressed as $(u_0, v_0) = \left[-xF'(r)/r, F(r)/r\right]$. Applying these definitions to Eq. (12), it may be shown that F must satisfy Yuan and Finkelstein's mean flow equation[33]

$$r^3F''' - 2r^2F'' + 3rF'' - 3F' + R\left[r^2(F'F'' - FF''') + r(3FF'' - F'^2) - 3FF'\right] = 0 \tag{14}$$

with

$$F'(1) = F'(0) = \lim_{r\to 0}(F'' - F'/r)/r = 0\,,\ F(1) = 1\,. \tag{15}$$

The mean pressure associated with F may be extracted through straightforward integration of Eq. (12); one gets

$$p_0(x,r) = 1/\gamma - \tfrac{1}{2}M^2r^{-2}\left[F^2 + x^2\left(F'^2 - FF'' + FF'/r\right)\right]. \tag{16}$$

3. Time Dependent Equations

Collecting terms of $\mathcal{O}(\bar{\varepsilon})$ from Eqs. (6)-(7) leads to

$$-i\omega\rho_1 + \nabla\cdot\boldsymbol{u}_1 = -M\nabla\cdot(\rho_1\boldsymbol{u}_0)\,, \tag{17}$$

$$-i\omega\boldsymbol{u}_1 = -M\left[\nabla(\boldsymbol{u}_0\cdot\boldsymbol{u}_1) - \boldsymbol{u}_1\times(\nabla\times\boldsymbol{u}_0) - \boldsymbol{u}_0\times(\nabla\times\boldsymbol{u}_1)\right] - \nabla p_1 + M\varepsilon\left[4\nabla(\nabla\cdot\boldsymbol{u}_1)/3 - \nabla\times(\nabla\times\boldsymbol{u}_1)\right]. \tag{18}$$

Equations (17) and (18) clearly suggest that the steady-state velocity $\boldsymbol{u}_0$ has a substantial bearing on the oscillatory flow component. This also emphasizes the role that Berman's class of mean flow solutions plays in modeling the oscillatory motion in porous channels and tubes.

C. Temporal Field Decomposition

In order to proceed, the temporal disturbances are now split into solenoidal and irrotational components. Using a circumflex to denote the curl-free pressure-driven part, and a tilde for the divergence-free boundary-driven part, the time-dependent velocity component may be expressed as

$$\boldsymbol{u}_1 = \hat{\boldsymbol{u}} + \tilde{\boldsymbol{u}} \tag{19}$$

with

$$\nabla\times\boldsymbol{u}_1 = \nabla\times\tilde{\boldsymbol{u}}\,,\ p_1 = \hat{p}\,,\ \rho_1 = \hat{\rho}\,. \tag{20}$$

This so-called Helmholtz decomposition charges all vortices to the solenoidal field and compressibility sources and sinks to the irrotational field.

Insertion of Eqs. (19)-(20) into Eqs. (17)-(18) leads to two independent sets that are coupled only through existing boundary conditions. The acoustic set remains compressible and irrotational while the vortical set combines both incompressible and rotational characteristics.

The Acoustic Set:

$$-i\omega\hat{\rho}+\nabla\cdot\hat{\boldsymbol{u}}=-M\nabla\cdot\left(\hat{\rho}\boldsymbol{u}_0\right), \tag{21}$$

$$-i\omega\hat{\boldsymbol{u}}=-\nabla\hat{p}+4M\varepsilon\nabla\left(\nabla\cdot\hat{\boldsymbol{u}}\right)/3-M\left[\nabla\left(\hat{\boldsymbol{u}}\cdot\boldsymbol{u}_0\right)-\hat{\boldsymbol{u}}\times\left(\nabla\times\boldsymbol{u}_0\right)\right]. \tag{22}$$

The Vortical Set:

$$\nabla\cdot\tilde{\boldsymbol{u}}=0, \tag{23}$$

$$-i\omega\tilde{\boldsymbol{u}}=-M\varepsilon\nabla\times\left(\nabla\times\tilde{\boldsymbol{u}}\right)-M\left[\nabla\left(\tilde{\boldsymbol{u}}\cdot\boldsymbol{u}_0\right)-\tilde{\boldsymbol{u}}\times\left(\nabla\times\boldsymbol{u}_0\right)-\boldsymbol{u}_0\times\left(\nabla\times\tilde{\boldsymbol{u}}\right)\right]. \tag{24}$$

Physically, two boundary conditions must be secured by the unsteady velocity component $\boldsymbol{u}_1$. These are the no-slip condition at the wall $u_1(x,1)=0$, and symmetry about the midsection plane, $\partial u_1(x,0)/\partial r=0$.

1. Acoustic Solution

Equation (21) can be multiplied by $-i\omega$ and added to the divergence of Eq. (22). After assuming that the system is isentropic to first order in the pressure wave amplitude, a wave equation is produced, namely,

$$\nabla^2\hat{p}+\omega^2\hat{p}=4M\varepsilon\nabla^2\left(\nabla\cdot\hat{\boldsymbol{u}}\right)/3-M\left\{i\omega\nabla\cdot\left(\boldsymbol{u}_0\hat{p}\right)+\nabla^2\left(\hat{\boldsymbol{u}}\cdot\boldsymbol{u}_0\right)-\nabla\cdot\left[\hat{\boldsymbol{u}}\times\left(\nabla\times\boldsymbol{u}_0\right)\right]\right\}. \tag{25}$$

A solution, at $\mathcal{O}(M)$, can be achieved through the use of separation of variables. Its construction assumes longitudinal oscillations and proceeds from the rigid wall boundary conditions. After some algebra, the acoustic pressure and velocity are found to be

$$\hat{p}=\cos\left(\omega x\right)+\mathcal{O}(M),\quad \hat{\boldsymbol{u}}=i\sin\left(\omega x\right)\hat{e}_x+\mathcal{O}(M). \tag{26}$$

2. Vortical Equations

Given that the ratio of the normal to axial velocity is of the same order as the Mach number (i.e. $\tilde{v}/\tilde{u}=\mathcal{O}(M)$), $\tilde{v}$ can be neglected at the first perturbation order. This assumption can be justified in view of the arguments presented by Majdalani and Van Moorhem.[45] Applying this condition, along with the definition of the mean flow velocity, the axial momentum equation reduces to

$$iS\tilde{u}=\frac{\partial}{\partial x}\left(\tilde{u}u_0\right)+v_0\frac{\partial\tilde{u}}{\partial r}-\frac{\varepsilon}{r}\frac{\partial}{\partial r}\left(r\frac{\partial\tilde{u}}{\partial r}\right)+\mathcal{O}(M), \tag{27}$$

where $S\equiv\omega/M$ is the Strouhal number. Having defined the mean flow stream function, Eq. (27) becomes

$$\left(iS+\frac{F'}{r}\right)\tilde{u}=\frac{F}{r}\frac{\partial\tilde{u}}{\partial r}-\frac{xF'}{r}\frac{\partial\tilde{u}}{\partial x}-\frac{\varepsilon}{r}\frac{\partial}{\partial r}\left(r\frac{\partial\tilde{u}}{\partial r}\right)+\mathcal{O}(M). \tag{28}$$

The next section presents further simplifications of Eq. (28).

3. The Separable Boundary-Layer Equation

A solution to Eq. (28) can be achieved through the use of separation of variables. Assuming the product

$$\tilde{u}\left(x,r\right)=X(x)Y(r), \tag{29}$$

substitution into Eq. (28) leads to

$$\frac{x}{X}\frac{\mathrm{d}X}{\mathrm{d}x}=\frac{F}{F'Y}\frac{\mathrm{d}Y}{\mathrm{d}r}-\frac{\varepsilon r}{F'Y}\frac{\mathrm{d}^2Y}{\mathrm{d}r^2}-\frac{\varepsilon}{F'Y}\frac{\mathrm{d}Y}{\mathrm{d}r}-\frac{iSr}{F'}-1=\kappa_n, \tag{30}$$

where $\kappa_n>0$ is the separation eigenvalue. The x-integral can be performed easily and then inserted into Eq. (29). The solution becomes

$$\tilde{u}(x,r)=\sum_n c_n x^{\kappa_n}Y_n(r), \tag{31}$$

where c_n is a constant associated with κ_n. Satisfaction of the no-slip boundary condition at the wall requires setting the acoustic and vortical velocity components equal and opposite at $r=1$. One finds

$$\tilde{u}(x,1)=-i\sin(\omega x). \tag{32}$$

At this point, one may use a series expansion of the sine function and set the result equal to Eq. (31); one obtains

$$\sum_n c_n x^{\kappa_n}Y_n(1)=-i\sum_{n=0}^{\infty}\frac{(-1)^n(\omega x)^{2n+1}}{(2n+1)!}. \tag{33}$$

Equating like-terms yields

$$\kappa_n = 2n+1,\ c_n = -i\frac{(-1)^n \omega^{2n+1}}{(2n+1)!},\ Y_n(1) = 1, \tag{34}$$

where $n = 0,1,2,...,\infty$. The expression for the rotational component emerges, namely,

$$\tilde{u}(x,r) = -i\sum_{n=0}^{\infty}\frac{(-1)^n(\omega x)^{2n+1}}{(2n+1)!}Y_n(r). \tag{35}$$

In order to complete Eq. (35), Y_n needs to be determined from Eq. (30). The search for Y_n leads to a boundary-value problem of the form

$$\varepsilon\frac{\mathrm{d}^2 Y_n}{\mathrm{d}r^2} + \left(-\frac{F}{r} + \frac{\varepsilon}{r}\right)\frac{\mathrm{d}Y_n}{\mathrm{d}r} + \left[iS + (2n+2)\frac{F'}{r}\right]Y_n = 0, \tag{36}$$

that is subject to

$$Y_n(1) = 1,\ \ Y_n'(0) = 0. \tag{37}$$

The two boundary conditions stem from the no slip and core symmetry requirements.

D. Boundary Layer Analysis

Equation (36), referred to as the separated momentum equation, is a linear ODE that can be represented by the general second order form

$$\varepsilon\frac{\mathrm{d}^2 G}{\mathrm{d}\eta^2} + a(\eta)\frac{\mathrm{d}G}{\mathrm{d}\eta} + \left[b(\eta) + iSc(\eta)\right]G = 0 \tag{38}$$

with

$$G(1) = 1 \text{ and } G'(0) = 0, \tag{39}$$

and where $a(\eta) = a_0(\eta) + \varepsilon a_1(\eta)$ and $b(\eta) = b_0(\eta) + \varepsilon b_1(\eta)$. For the suction case, $a(\eta) \le 0$, whereas $b(\eta)$ and $c(\eta)$ will be positive throughout the solution domain.

The mathematical treatment of Eq. (38) may be achieved through the use of classic perturbation techniques. For this purpose, a small perturbation parameter must first be defined. From a physical standpoint, we must insist that fluid withdrawal at the surface can play an appreciable role in altering the flowfield associated with non-porous channels and tubes. We thus conclude that the crossflow Reynolds number must be finite and that $\varepsilon < 1$. Additionally, in order to develop an oscillatory flow that is markedly different from the mean flow, the Strouhal number must be sufficiently large or $S > 1$.

Asymptotic approximations to the solution of Eq. (38) will subsequently depend on the development of a relation between the two possible perturbation parameters that characterize this problem. By inspection of the exact solutions developed for the infinite suction case, and by scrutinizing numerical solutions developed for small suction, we realize that the problem exhibits a typical second-order wave type response that tends to be slightly under-damped (i.e., with minimal overshoot) over all ranges of ε and S. Consequently, the assumption that Eq. (38) leads to a critically damped response will be adopted in relating the small perturbation parameter (ε) to the large perturbation parameter (S).

To begin, a generic relation between the flow parameters is assumed:

$$S \sim \varepsilon^{-\zeta}. \tag{40}$$

Then to ensure that the derivatives are of $\mathcal{O}(1)$, the independent coordinate can be stretched by means of

$$\eta = \varepsilon^k \chi. \tag{41}$$

At this stage, the substitution of Eqs. (40)-(41) into Eq. (38) give rise to

$$\varepsilon\varepsilon^{-2k}\frac{\mathrm{d}^2 G}{\mathrm{d}\chi^2} + \varepsilon^{-k}a(\eta)\frac{\mathrm{d}G}{\mathrm{d}\chi} + \left[b(\eta) + i\varepsilon^{-\zeta}c(\eta)\right]G = 0. \tag{42}$$

The resulting expression clearly displays the orders of magnitude of each of its members. For a critically damped response to occur, a balance between all three terms in Eq. (42) must be established. Such a paradigm will require that $\zeta = k$ and so

$$\varepsilon^{1-2\zeta}\frac{\mathrm{d}^2 G}{\mathrm{d}\chi^2} + \varepsilon^{-\zeta}a(\eta)\frac{\mathrm{d}G}{\mathrm{d}\chi} + \left[b(\eta) + i\varepsilon^{-\zeta}c(\eta)\right]G = 0. \tag{43}$$

Balancing terms in Eq. (43) yields $\zeta = 1$ for the suction case. Its unique distinguished limit is therefore identified as $S \sim \varepsilon^{-1}$. While other distinguished limits of the type $S \sim \varepsilon^{-1/2}$, $S \sim \varepsilon^{-1/3}$, etc., may be used with limitations in the injection-driven flow analogue, they lead to unphysical solutions for the case at hand.

III. Generalized Asymptotic Solutions

Attempts are made here to apply classic perturbation techniques to solve Eq. (38) in its general representation. To do so, a two-variable multiple-scales solution to the problem is presented after extrapolating the relevant inner variable from a formal scaling analysis. This is followed by a WKB expansion in which the solution is assumed to possess, as it should, an exponential damping character. At the heart of each solution will be the reduction of the attendant doubly-perturbed equation of motion into a singly-perturbed relation. This, in turn, will be accomplished through the judicious choice of an asymptotic relation linking the two existing group parameters.

A. Generalized Multiple-Scales Solution

It is known that the validity of multiple-scales analysis is closely tied to the choice of inner scales. Herein, the inner coordinate transformation may rest on stretching the independent variable by ε. With the boundary layer developing near the wall ($\eta = 1$), we introduce two scales of the form

$$\eta = \eta \quad \text{and} \quad \chi = \frac{1-\eta}{\varepsilon}. \tag{44}$$

In the above, η denotes the outer scale while χ designates the stretched coordinate inside the boundary layer.

1. Leading-Order Multiple-Scales Expansion

Application of the inner variable transformation to Eq. (38) leads to

$$\frac{\mathrm{d}^2 G}{\mathrm{d}\chi^2} - \left[a_0(\eta) + \varepsilon a_1(\eta)\right]\frac{\mathrm{d}G}{\mathrm{d}\chi} + \varepsilon\left[b_0(\eta) + \varepsilon b_1(\eta) + iSc(\eta)\right]G = 0. \tag{45}$$

Recalling that G depends on both scales, derivatives are converted into

$$\frac{\mathrm{d}G}{\mathrm{d}\chi} = \frac{\partial G}{\partial \chi} - \varepsilon\frac{\partial G}{\partial \eta} \text{ and } \frac{\mathrm{d}^2 G}{\mathrm{d}\chi^2} = \frac{\partial^2 G}{\partial \chi^2} - 2\varepsilon\frac{\partial^2 G}{\partial \eta \partial \chi} + \mathcal{O}(\varepsilon^2). \tag{46}$$

Now letting $G = G_0 + \varepsilon G_1 + \mathcal{O}(\varepsilon^2)$, Eq. (45) becomes

$$\frac{\partial^2 G_0}{\partial \chi^2} + \varepsilon\frac{\partial^2 G_1}{\partial \chi^2} - 2\varepsilon\frac{\partial^2 G_0}{\partial \eta \partial \chi} - \left(a_0 + \varepsilon a_1\right)\frac{\partial G_0}{\partial \chi} - \varepsilon\left(a_0 + \varepsilon a_1\right)\frac{\partial G_1}{\partial \chi}$$
$$+\varepsilon\left(a_0 + \varepsilon a_1\right)\frac{\partial G_0}{\partial \eta} + \varepsilon\left(b_0 + \varepsilon b_1 + iSc\right)\left(G_0 + \varepsilon G_1\right) = 0. \tag{47}$$

At this stage, two equations may be segregated for G_0 and G_1. With the assumption that $S \sim \varepsilon^{-1}$, the $\mathcal{O}(1)$ expression returns

$$\frac{\partial^2 G_0}{\partial \chi^2} - a_0\frac{\partial G_0}{\partial \chi} + iSc\varepsilon G_0 = 0, \tag{48}$$

and at $\mathcal{O}(\varepsilon)$,

$$\frac{\partial^2 G_1}{\partial \chi^2} - a_0\frac{\partial G_1}{\partial \chi} + iSc\varepsilon G_1 = 2\frac{\partial^2 G_0}{\partial \eta \partial \chi} + a_1\frac{\partial G_0}{\partial \chi} - a_0\frac{\partial G_0}{\partial \eta} - b_0 G_0. \tag{49}$$

Solving Eq. (48) yields

$$G_0 = A_1(\eta)\exp\left[\left(a_0 + \sqrt{a_0^2 - 4iSc\varepsilon}\right)\frac{\chi}{2}\right] + A_2(\eta)\exp\left[\left(a_0 - \sqrt{a_0^2 - 4iSc\varepsilon}\right)\frac{\chi}{2}\right]. \tag{50}$$

Forthwith, Eq. (50) may be differentiated and inserted into the right-hand-side of Eq. (49). Then the principle of least singular behavior may be called upon to prevent the emergence of secular terms at $\mathcal{O}(\varepsilon)$. The desired condition can be achieved by putting

$$\frac{\mathrm{d}A_1}{\mathrm{d}\eta} = \left[\frac{\left(2b_0 - 2a_0' - a_0 a_1\right)\sqrt{a_0^2 - 4iSc\varepsilon} - 2a_0 a_0' + 4iSc'\varepsilon - a_1\left(a_0^2 - 4iSc\varepsilon\right)}{2\left(a_0^2 - 4iSc\varepsilon\right)}\right]A_1, \tag{51}$$

and

$$\frac{\mathrm{d}A_2}{\mathrm{d}\eta}=\left[\frac{\left(2a_0'-2b_0+a_0a_1\right)\sqrt{a_0^2-4iSc\varepsilon}-2a_0a_0'+4iSc'\varepsilon-a_1\left(a_0^2-4iSc\varepsilon\right)}{2\left(a_0^2-4iSc\varepsilon\right)}\right]A_2\,, \tag{52}$$

where primes denote differentiation with respect to η. The solutions to Eqs. (51)-(52) may then be substituted into Eq. (50) to give

$$G_0=c_1\exp\left\{I_1+\left(a_0+\sqrt{a_0^2-4iSc\varepsilon}\right)\frac{(1-\eta)}{2\varepsilon}\right\}+c_2\exp\left\{I_2+\left(a_0-\sqrt{a_0^2-4iSc\varepsilon}\right)\frac{(1-\eta)}{2\varepsilon}\right\} \tag{53}$$

with

$$I_1=\int_1^{\eta}\left[\frac{\left(2b_0-2a_0'-a_0a_1\right)\sqrt{a_0^2-4iSc\varepsilon}-2a_0a_0'+4iSc'\varepsilon-a_1\left(a_0^2-4iSc\varepsilon\right)}{2\left(a_0^2-4iSc\varepsilon\right)}\right]\mathrm{d}z\,, \tag{54}$$

$$I_2=\int_1^{\eta}\left[\frac{\left(2a_0'-2b_0+a_0a_1\right)\sqrt{a_0^2-4iSc\varepsilon}-2a_0a_0'+4iSc'\varepsilon-a_1\left(a_0^2-4iSc\varepsilon\right)}{2\left(a_0^2-4iSc\varepsilon\right)}\right]\mathrm{d}z\,. \tag{55}$$

Note that c_1 and c_2 are pure constants connected with the boundary conditions. In fact, the constraints $G_0(1)=1$ and $G_0'(0)=0$ may be applied along with the assumption that $c(0)>0$ to produce

$$c_1=0 \quad \text{and} \quad c_2=1\,. \tag{56}$$

Finally, the generalized multiple-scales solution that we arrive at can be expressed as

$$G=\exp\left\{I_2+\left(a_0-\sqrt{a_0^2-4iSc\varepsilon}\right)\frac{(1-\eta)}{2\varepsilon}\right\}. \tag{57}$$

2. Leading-Order Eigensolution

For arbitrary suction profiles at the wall, the generic parameters in Eq. (38) become

$$G=Y_n\,,\ \eta=r\,,\ a_0=-F/r\,,\ a_1=1/r\,,\ b_0=(2n+2)F'/r\,,\ b_1=0\,,\text{ and }\ c=1 \tag{58}$$

Using these definitions along with Eqs. (57) and (55), the leading-order expression for Y_n may be written as

$$Y_n=\exp\left\{I_2+\left(Fr^{-1}+\sqrt{F^2r^{-2}-4iS\varepsilon}\right)\frac{(r-1)}{2\varepsilon}\right\} \tag{59}$$

where

$$I_2=\int_1^r\frac{Fz^{-1}\left(Fz^{-2}-F'z^{-1}\right)}{F^2z^{-2}-4iS\varepsilon}\mathrm{d}z-\frac{1}{2}\int_1^r\frac{\mathrm{d}z}{z}+(2n+3)\int_1^r\frac{Fz^{-2}-F'z^{-1}}{\sqrt{F^2z^{-2}-4iS\varepsilon}}\mathrm{d}z\ -\left(2n+\tfrac{5}{2}\right)\int_1^r\frac{Fz^{-2}}{\sqrt{F^2z^{-2}-4iS\varepsilon}}\mathrm{d}z \tag{60}$$

and $F_0=F(1)$. It may be worthwhile to remark that I_2 consists of a higher-order correction in Eq. (59). Furthermore, the first three members of Eq. (60) may be integrated in terms of the general mean flow function F. Although the fourth term cannot be explicitly integrated, it represents a secondary contribution that does not affect the solution at $\mathcal{O}(\varepsilon)$. For this reason, only the leading eigenvalue $(n=0)$ will be essential. Integrating and applying the definite bounds renders a nearly closed-form approximation for Y_n, namely,

$$Y_n=\left[\frac{r\left(F_0+\sqrt{F_0^2-4iS\varepsilon}\right)}{F+\sqrt{F^2-4iS\varepsilon r^2}}\right]^{2n+3}\left[\frac{r\left(F_0^2-4iS\varepsilon\right)}{F^2-4iS\varepsilon r^2}\right]^{\frac{1}{2}}\exp\left[\left(Fr^{-1}+\sqrt{F^2r^{-2}-4iS\varepsilon}\right)\frac{(r-1)}{2\varepsilon}\ -\frac{5}{2}\int_1^r\frac{Fz^{-2}}{\sqrt{F^2z^{-2}-4iS\varepsilon}}\mathrm{d}z\right]. \tag{61}$$

It may be easily verified that the resulting formulation stands in excellent agreement with the numerical solution of Eq. (36). In practice, when compared over the parametric range associated with plausible physical settings, numerics and asymptotics become indiscernible.

3. Axial Velocity in Multiple Scales

Pursuant to the flowfield decomposition presented earlier, the unsteady axial wave velocity may be synthesized from $u_1=\hat{u}+\tilde{u}$ with $\hat{u}=i\sin(\omega x)$ standing for the acoustic wave. The vortical wave that suitably cancels with $\hat{u}$ at the wall may be cast into

$$\tilde{u}(x,r) = -i\sum_{n=0}^{\infty} \frac{(-1)^n (\omega x)^{2n+1}}{(2n+1)!} Y_n(r) \tag{62}$$

Given the availability of an explicit Y_n, the axially traveling wave velocity can be assembled into

$$u_1(x,r) = i\left\{ \sin(\omega x) - \exp\left[\left(Fr^{-1} + \sqrt{F^2 r^{-2} - 4iS\varepsilon} \right) \frac{(r-1)}{2\varepsilon} - \frac{5}{2}\int_1^r \frac{Fz^{-2}}{\sqrt{F^2 z^{-2} - 4iS\varepsilon}} \mathrm{d}z \right] \right.$$
$$\left. \times \left[\frac{r\left(F_0 + \sqrt{F_0^2 - 4iS\varepsilon}\right)}{F + \sqrt{F^2 - 4iS\varepsilon r^2}} \right]^2 \left[\frac{r\left(F_0^2 - 4iS\varepsilon\right)}{F^2 - 4iS\varepsilon r^2} \right]^{\frac{1}{2}} \sin\left[\frac{\omega x r\left(F_0 + \sqrt{F_0^2 - 4iS\varepsilon}\right)}{F + \sqrt{F^2 - 4iS\varepsilon r^2}} \right] \right\} \tag{63}$$

Driven by the accuracy associated with Y_n, $u_1(x,r)$ may be tested and shown to provide an excellent approximation vis-à-vis numerical simulations of this problem.

B. Generalized WKB Solution

For an *n*th order linear ODE that exhibits an oscillatory behavior, a traditional WKB expansion assumes that G possesses *n* linearly-independent solutions of the form

$$G \sim \exp\left[\frac{1}{\delta} \sum_{j=0}^{\infty} \delta^j Q_j \right], \tag{64}$$

where

$$G' \sim \left[\frac{1}{\delta} \sum_{j=0}^{\infty} \delta^j Q_j' \right] \exp\left[\frac{1}{\delta} \sum_{j=0}^{\infty} \delta^j Q_j \right] \text{ and } G'' \sim \left[\frac{1}{\delta^2} \left(\sum_{j=0}^{\infty} \delta^j Q_j' \right)^2 + \frac{1}{\delta} \sum_{j=0}^{\infty} \delta^j Q_j'' \right] \exp\left[\frac{1}{\delta} \sum_{j=0}^{\infty} \delta^j Q_j \right]. \tag{65}$$

1. Leading-Order WKB Expansion

Substituting Eqs. (64)-(65) into Eq. (38) and rearranging, one gets,

$$\frac{\varepsilon}{\delta^2} \left(\sum_{j=0}^{\infty} \delta^j Q_j' \right)^2 + \frac{\varepsilon}{\delta} \sum_{j=0}^{\infty} \delta^j Q_j'' + \frac{a_0}{\delta} \sum_{j=0}^{\infty} \delta^j Q_j' + \frac{a_1 \varepsilon}{\delta} \sum_{j=0}^{\infty} \delta^j Q_j' + b_0 + \varepsilon b_1 + iSc = 0. \tag{66}$$

Subsequent expansion to the order of Q_1 gives

$$\frac{\varepsilon}{\delta^2} Q_0'^2 + \frac{2\varepsilon}{\delta} Q_0' Q_1' + \varepsilon Q_1'^2 + \frac{\varepsilon}{\delta} Q_0'' + \varepsilon Q_1'' + \frac{a_0}{\delta} Q_0' + a_0 Q_1' + \frac{a_1 \varepsilon}{\delta} Q_0' + a_1 \varepsilon Q_1' + b_0 + \varepsilon b_1 + iSc = 0. \tag{67}$$

Using the assumptions of a critically damped response and $S \sim \varepsilon^{-1}$, δ may be determined such that dominant terms acquire equal weights. Balancing the leading-order terms in Eq. (38) swiftly yields $\delta = \varepsilon$. This enables us to change Eq. (67) into

$$\frac{1}{\varepsilon} Q_0'^2 + 2Q_0' Q_1' + Q_0'' + \frac{a_0}{\varepsilon} Q_0' + a_0 Q_1' + a_1 Q_0' + b_0 + iSc + \mathcal{O}(\varepsilon) = 0. \tag{68}$$

From Eq. (68), two equations can be retrieved for Q_0 and Q_1. At $\mathcal{O}(1/\varepsilon)$, one finds the so-called Eikonal equation,

$$Q_0'^2 + a_0 Q_0' + iSc\varepsilon = 0, \tag{69}$$

and at $\mathcal{O}(1)$, one extracts the transport equation,

$$Q_1' = \frac{-\left(Q_0'' + b_0 + a_1 Q_0'\right)}{\left(2Q_0' + a_0\right)}. \tag{70}$$

The solution of Eq. (69) engenders dual solutions, specifically

$$Q_0 = \frac{1}{2}\int_1^{\eta} \left(\pm\sqrt{a_0^2 - 4iSc\varepsilon} - a_0 \right) \mathrm{d}z. \tag{71}$$

A leading-order WKB approximation can be constructed now from the linear combination of the two explicit roots of Eq. (71). One obtains

$$G = c_1 \exp\left[\frac{1}{2\varepsilon} \int_1^{\eta} \left(\sqrt{a_0^2 - 4iSc\varepsilon} - a_0 \right) \mathrm{d}z \right] + c_2 \exp\left[\frac{-1}{2\varepsilon} \int_1^{\eta} \left(\sqrt{a_0^2 - 4iSc\varepsilon} + a_0 \right) \mathrm{d}z \right]. \tag{72}$$

Equation (72) can be paired with $G(1)=1$ and $G'(0)=0$ to secure

$$c_1 = \frac{\exp\left[\frac{-1}{2\varepsilon}\int_1^0\left(\sqrt{a_0^2-4iSc\varepsilon}+a_0\right)\mathrm{d}z\right]}{\exp\left[\frac{-1}{2\varepsilon}\int_1^0\left(\sqrt{a_0^2-4iSc\varepsilon}+a_0\right)\mathrm{d}z\right]-\exp\left[\frac{1}{2\varepsilon}\int_1^0\left(\sqrt{a_0^2-4iSc\varepsilon}-a_0\right)\mathrm{d}z\right]}, \tag{73}$$

and

$$c_2 = \frac{\exp\left[\frac{1}{2\varepsilon}\int_1^0\left(\sqrt{a_0^2-4iSc\varepsilon}-a_0\right)\mathrm{d}z\right]}{\exp\left[\frac{1}{2\varepsilon}\int_1^0\left(\sqrt{a_0^2-4iSc\varepsilon}+a_0\right)\mathrm{d}z\right]-\exp\left[\frac{-1}{2\varepsilon}\int_1^0\left(\sqrt{a_0^2-4iSc\varepsilon}-a_0\right)\mathrm{d}z\right]}. \tag{74}$$

For the wall suction case, recalling that $c(\eta)>0$ throughout the fluid domain, Eqs. (73) and (74) may be shown to reproduce $c_1=1$ and $c_2=0$ as $\varepsilon\to 0$.

2. Two-Term WKB Approximation

Solving to $\mathcal{O}(\varepsilon)$ can be achieved through the direct integration of Eq. (70) viz.

$$Q_1 = -\int_1^\eta \frac{\left(Q_0''+b_0+a_1Q_0'\right)}{\left(2Q_0'+a_0\right)}\,\mathrm{d}z\,. \tag{75}$$

The integrand contains Q_0 and so we choose the right-traveling wave solution presented in Eq. (71). By selecting

$$Q_0 = \frac{1}{2}\int_1^\eta\left(\sqrt{a_0^2-4iSc\varepsilon}-a_0\right)\mathrm{d}z\,, \tag{76}$$

Eq. (75) reduces to

$$Q_1 = \frac{1}{2}\left(\int_1^\eta \frac{a_0'+a_0a_1-2b_0}{\sqrt{a_0^2-4iSc\varepsilon}}\,\mathrm{d}z-\int_1^\eta\frac{a_0a_0'}{a_0^2-4iSc\varepsilon}\,\mathrm{d}z-\int_1^\eta a_1\mathrm{d}z\right). \tag{77}$$

Both Q_0 and Q_1 may be consolidated into

$$G = \exp\left[\frac{1}{2\varepsilon}\int_1^\eta\left(\sqrt{a_0^2-4iSc\varepsilon}-a_0\right)\mathrm{d}z+\frac{1}{2}\left(\int_1^\eta\frac{a_0'+a_0a_1-2b_0}{\sqrt{a_0^2-4iSc\varepsilon}}\,\mathrm{d}z-\int_1^\eta\frac{a_0a_0'}{a_0^2-4iSc\varepsilon}\,\mathrm{d}z-\int_1^\eta a_1\mathrm{d}z\right)\right]. \tag{78}$$

3. WKB Eigensolution

Substituting the place-holding coefficients from Eq. (58) into Eq. (78), a leading-order WKB solution for arbitrary F may be constructed. We get

$$Y_n = \exp\left[\frac{1}{2\varepsilon}\int_1^r\left(\sqrt{F^2z^{-2}-4iS\varepsilon}+Fz^{-1}\right)\mathrm{d}z-\frac{1}{2}\int_1^r\frac{Fz^{-1}\left(F'z^{-1}-Fz^{-2}\right)}{F^2z^{-2}-4iS\varepsilon}\,\mathrm{d}z-\frac{1}{2}\int_1^r\frac{\mathrm{d}z}{z}\right.$$
$$\left.-\left(2n+\tfrac{5}{2}\right)\int_1^r\frac{F'z^{-1}-Fz^{-2}}{F^2z^{-2}-4iS\varepsilon}\,\mathrm{d}z-\left(2n+\tfrac{5}{2}\right)\int_1^r\frac{Fz^{-2}}{F^2z^{-2}-4iS\varepsilon}\,\mathrm{d}z\right]. \tag{79}$$

In Eq. (79) only the first and last members in the exponential cannot be tacitly integrated and hence expressed directly in terms of F. While the first term must be retained, the last can be approximated at $\mathcal{O}(\varepsilon)$. This is accomplished by keeping the first eigenvalue associated with $n=0$ in that term only. We hence arrive at

$$Y_n = \left[\frac{r\left(F_0+\sqrt{F_0^2-4iS\varepsilon}\right)}{F+\sqrt{F^2-4iS\varepsilon r^2}}\right]^{2n+\frac{5}{2}}\left(\frac{F_0^2-4iS\varepsilon}{F^2-4iS\varepsilon r^2}\right)^{\frac{1}{4}}\exp\left[\frac{1}{2\varepsilon}\int_1^r\left(\sqrt{F^2z^{-2}-4iS\varepsilon}+Fz^{-1}\right)\mathrm{d}z-\frac{5}{2}\int_1^r\frac{Fz^{-2}}{F^2z^{-2}-4iS\varepsilon}\,\mathrm{d}z\right]. \tag{80}$$

4. Axial Velocity in WKB

Equation (80) may be inserted into the axial traveling wave expression to produce

$$u_1(x,r) = i\left\{\sin(\omega x)-\exp\left[\frac{1}{2\varepsilon}\int_1^r\left(\sqrt{F^2z^{-2}-4iS\varepsilon}+Fz^{-1}\right)\mathrm{d}z-\frac{5}{2}\int_1^r\frac{Fz^{-2}}{F^2z^{-2}-4iS\varepsilon}\,\mathrm{d}z\right]\right.$$

$$\times\left[\frac{r\left(F_0+\sqrt{F_0^2-4iS\varepsilon}\right)}{F+\sqrt{F^2-4iS\varepsilon r^2}}\right]^{\frac{3}{2}}\left(\frac{F_0^2-4iS\varepsilon}{F^2-4iS\varepsilon r^2}\right)^{\frac{1}{4}}\sin\left[\frac{\omega x r\left(F_0+\sqrt{F_0^2-4iS\varepsilon}\right)}{F+\sqrt{F^2-4iS\varepsilon r^2}}\right]\Bigg\} \tag{81}$$

The resulting formulation is comparable in accuracy to Eq. (63). However, unlike the multiple-scales approximation in which the first exponential argument may be obtained in closed form, the WKB equivalent requires the evaluation of the corresponding integral, $\int[(F^2z^{-2}-4iS\varepsilon)^{1/2}+Fz^{-1}]\mathrm{d}z$.

IV. Results

To demonstrate the accuracy of the expressions that may be recovered from the generalized multiple-scales and WKB analyses, our approximations are compared to an exact solution developed for $R\geq 20$.[37] For flow in a porous tube with large wall suction, the steady-state profile derived by Terrill and Thomas may be used, namely,[35]

$$F(r)=r^2\,. \tag{82}$$

Inserting this characteristic function into Eqs. (61) and (63), expressions for Y_n and u_1 from the multiple-scales analysis read

$$Y_n=\left[\frac{r+2(1-r)\sqrt{iS\varepsilon}-4iS\varepsilon}{r-2(1-r)\sqrt{iS\varepsilon}-4iS\varepsilon}\right]^{\frac{5}{8\sqrt{iS\varepsilon}}}\left[\frac{\left(1+\sqrt{1-4iS\varepsilon}\right)}{r+\sqrt{r^2-4iS\varepsilon}}\right]^{2n+3}\left(\frac{1-4iS\varepsilon}{r^3-4iS\varepsilon r}\right)^{\frac{1}{2}}\exp\left[\left(r+\sqrt{r^2-4iS\varepsilon}\right)\frac{(r-1)}{2\varepsilon}\right] \tag{83}$$

and

$$u_1(x,r)=i\Bigg\{\sin(\omega x)-\left[\frac{r+2(1-r)\sqrt{iS\varepsilon}-4iS\varepsilon}{r-2(1-r)\sqrt{iS\varepsilon}-4iS\varepsilon}\right]^{\frac{5}{8\sqrt{iS\varepsilon}}}\exp\left[\left(r+\sqrt{r^2-4iS\varepsilon}\right)\frac{(r-1)}{2\varepsilon}\right]$$
$$\times\left[\frac{\left(1+\sqrt{1-4iS\varepsilon}\right)}{r+\sqrt{r^2-4iS\varepsilon}}\right]^{2}\left(\frac{1-4iS\varepsilon}{r^3-4iS\varepsilon r}\right)^{\frac{1}{2}}\sin\left[\frac{\omega x\left(1+\sqrt{1-4iS\varepsilon}\right)}{r+\sqrt{r^2-4iS\varepsilon}}\right]\Bigg\}. \tag{84}$$

Along similar lines, the WKB solution for large suction may be deduced by placing Eq. (82) in Eqs. (80) and (81). These substitutions yield

$$Y_n=\left[\frac{r+2(1-r)\sqrt{iS\varepsilon}-4iS\varepsilon}{r-2(1-r)\sqrt{iS\varepsilon}-4iS\varepsilon}\right]^{\frac{5}{8\sqrt{iS\varepsilon}}}\left[\frac{\left(1+\sqrt{1-4iS\varepsilon}\right)}{r+\sqrt{r^2-4iS\varepsilon}}\right]^{\left(\frac{7}{2}+2n+iS\right)}\left(\frac{1-4iS\varepsilon}{r^4-4iS\varepsilon r^2}\right)^{\frac{1}{4}}$$
$$\times\exp\left[\frac{1}{4\varepsilon}\left(r\sqrt{r^2-4iS\varepsilon}-\sqrt{1-4iS\varepsilon}+r^2-1\right)\right] \tag{85}$$

and

$$u_1(x,r)=i\Bigg\{\sin(\omega x)-\left[\frac{r+2(1-r)\sqrt{iS\varepsilon}-4iS\varepsilon}{r-2(1-r)\sqrt{iS\varepsilon}-4iS\varepsilon}\right]^{\frac{5}{8\sqrt{iS\varepsilon}}}\exp\left[\frac{1}{4\varepsilon}\left(r\sqrt{r^2-4iS\varepsilon}-\sqrt{1-4iS\varepsilon}+r^2-1\right)\right]$$
$$\times\left[\frac{\left(1+\sqrt{1-4iS\varepsilon}\right)}{r+\sqrt{r^2-4iS\varepsilon}}\right]^{\left(\frac{3}{2}+iS\right)}\left(\frac{1-4iS\varepsilon}{r^4-4iS\varepsilon r^2}\right)^{\frac{1}{4}}\sin\left[\frac{\omega x\left(1+\sqrt{1-4iS\varepsilon}\right)}{r+\sqrt{r^2-4iS\varepsilon}}\right]\Bigg\}. \tag{86}$$

Finally, we can refer to Jankowski and Majdalani[37] who developed an exact solution for large suction in a tube. In the interest of clarity, their result may be expressed as

$$Y_n(r)=\frac{\Phi\left(-2n-2-\frac{1}{2}S,1;\frac{1}{2}Rr^2\right)}{\Phi\left(-2n-2-\frac{1}{2}S,1;\frac{1}{2}R\right)}, \tag{87}$$

and

$$u_1(x,r) = i\left[\sin(\omega x) - \sum_{n=0}^{\infty} \frac{(-1)^n (\omega x)^{2n+1} \Phi\left(-2n-2-\frac{1}{2}iS, 1; \frac{1}{2}Rr^2\right)}{(2n+1)!\,\Phi\left(-2n-2-\frac{1}{2}iS, 1; \frac{1}{2}R\right)}\right], \tag{88}$$

where $\Phi(a,b;z)$ denotes the confluent hypergeometric function.

Figure 2 presents a graphical evaluation of the exact and asymptotic solutions for Y_0. Over typical ranges of operating parameters, the graphical comparison shows that both the WKB and multiple-scales approximations stand in close agreement with the exact solution. One may also infer by inspection of part b that the accuracy of the asymptotic methods improves at higher Reynolds or Strouhal numbers. Furthermore, the slightly under-damped wave type response can be observed. This behavior is consistent with the original assumption that we made of a weakly under-damped response. The underlying conjecture played an important factor in generating an asymptotic relation between R and S that was essential for the development of both the multiple-scales and WKB approximations.

To more thoroughly quantify the accuracy of the attendant formulations, their error curves are displayed in Figs. 3a and 3b for the multiple-scales and WKB expansions, respectively. Therein, the maximum absolute error throughout the solution domain is plotted versus ε for the first three eigenmodes, $n = 0,1$ and 2. In both parts of the graph, the error is seen to diminish in absolute value with successive increases in S and R. Such behavior may

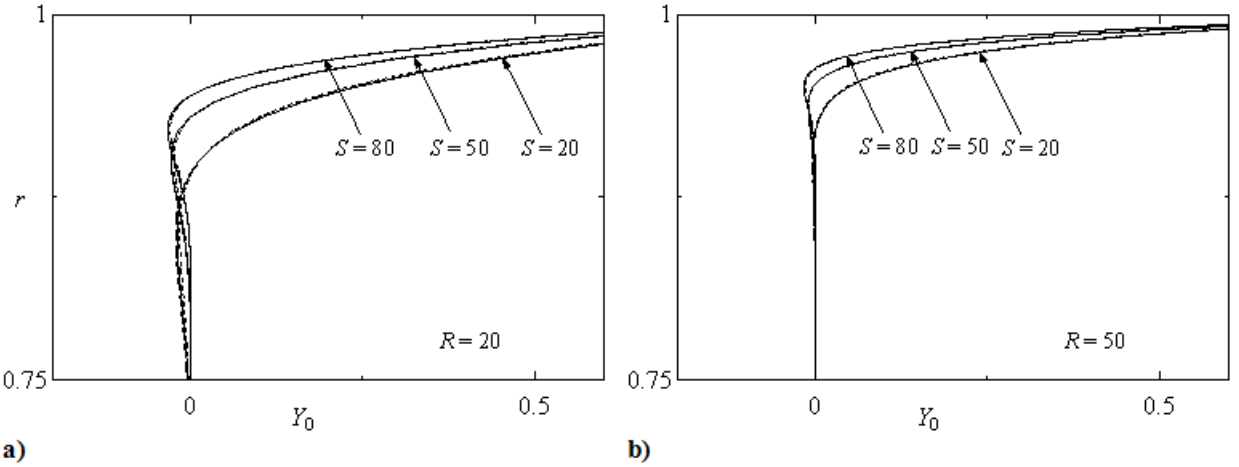

Figure 2. Graphical comparison of Y_0 for a) R=20 and b) R=50 over a range of S. The exact solution (solid line), multiple-scales (long dash), and WKB (short dash) are compared.

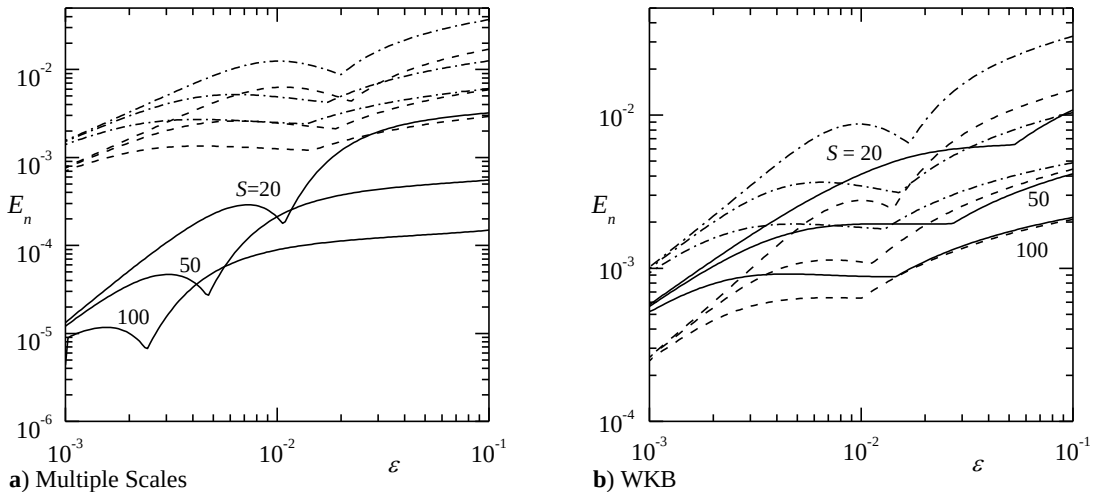

Figure 3. Maximum absolute error vs. ε for a) multiple-scales and b) WKB solutions using n=0 (solid), n=1 (dash), and n=2 (dot-dash).

be expected if one can recall that the analysis starts by perturbing the solution in the inverse of the Reynolds number and that an asymptotic relation linking S and R is assumed at the onset. Furthermore, one observes that the slopes of the curves for all three eigenvalues approach unity as $\varepsilon \to 0$, at high Reynolds number. The consistent convergence of the error curves into linear behavior provides a numerical confirmation of the reported asymptotic order associated with the derivation of Y_n at $\mathcal{O}(\varepsilon)$. One exception occurs in the multiple-scales approximation which, as shown in Fig. 3a (solid lines), exhibits a doubling in the error convergence rate for the $n = 0$ oscillation eigenmode.

In Fig. 4, the total unsteady longitudinal velocity is plotted at four separate times for the fundamental axial oscillation mode, $m = 1$. In this effort, the magnitude of the axially traveling wave is calculated at the chamber midpoint, $x/l = \frac{1}{2}$, using exact (solid line), multiple-scales (long dash) and WKB solutions (short dash). Only the real part of $u_1 \exp(-it)$ is shown in view of the un-physicality of the imaginary part. The ensuing graphical representations illustrate the striking resemblance established between the approximate models and the exact solutions that they represent over wide ranges of Reynolds and Strouhal numbers.

The oscillatory wave profiles in Fig. 4 depict a thin rotational layer near the wall and an irrotational region in the core. Furthermore, a velocity overshoot may be observed in the rotational layer near the wall. This near-wall overshoot, referred to as Richardson's annular effect, has been observed and extensively characterized for oscillatory flows in channels and tubes with impermeable walls.[40-42] In fact, the effect of doubling the oscillation

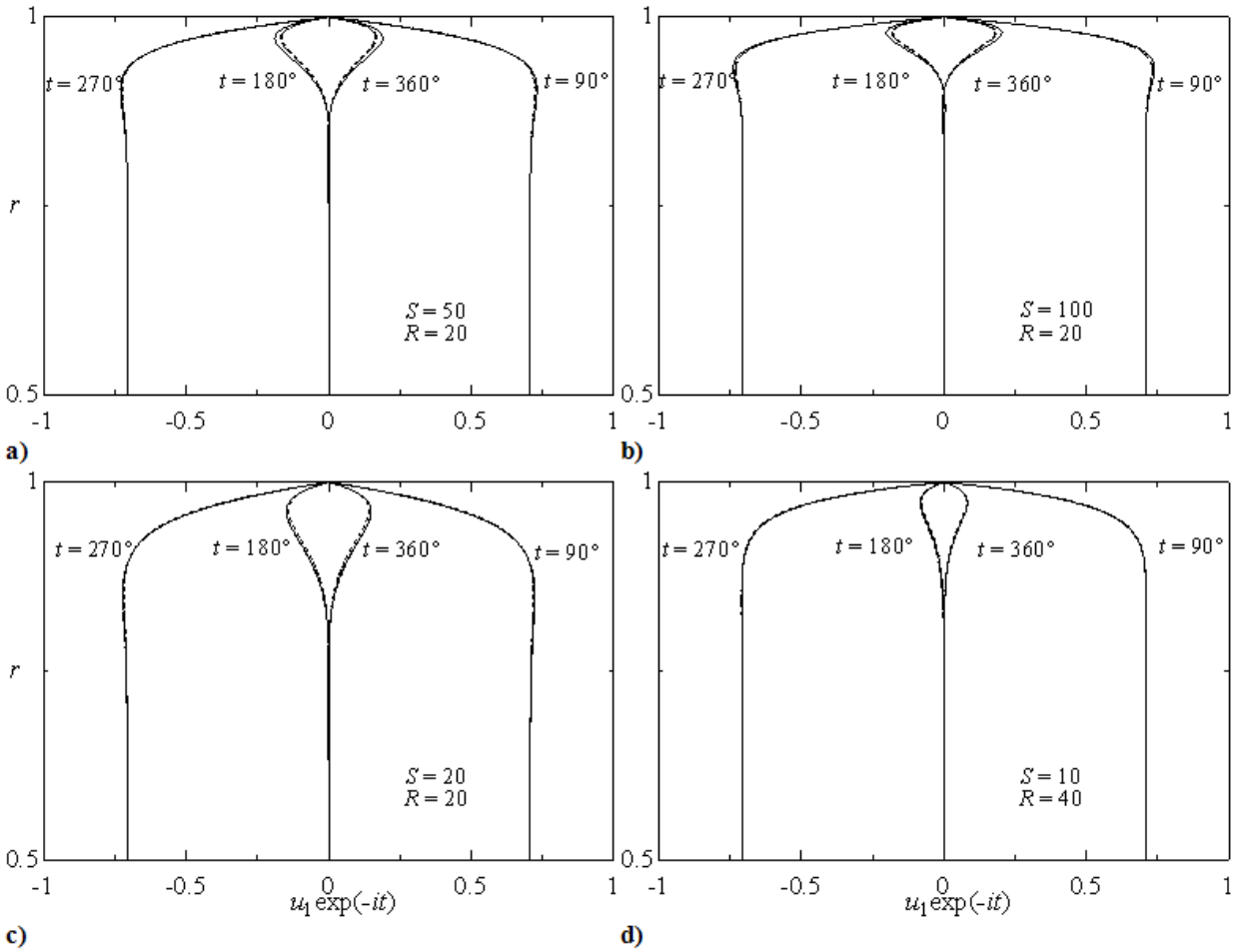

Figure 4. The axially traveling wave velocity, u_1 exp(–*it*), plotted at four different times. The oscillation frequency is doubled when going from a) to b), while the wall suction velocity is doubled when going from c) to d). The exact (solid line), multiple-scales (long dash), and WKB (short dash) solutions are plotted for *m*=1 and *x*/*l*=½.

frequency on the wave character is illustrated in Figs. 4a at $S = 50$ and 4b at $S = 100$ for a fixed suction velocity corresponding to $R = 20$. These figures show that increasing the oscillation frequency drives the location of the maximum unsteady velocity closer to the wall while simultaneously increasing the magnitude of the velocity overshoot. Both of these observations are in accord with the theory of time-dependent laminar flows.[46,47] They are also concurrent with the effect of increasing the Strouhal number on the injection-driven traveling wave analogue in porous tubes.[43,44] As for the impact of suction itself, Figs. 4c and 4d are used to showcase the effect of doubling the wall velocity. This is accomplished by increasing the Reynolds number from 20 to 40 while simultaneously reducing the Strouhal number from 20 to 10, because U_w appears in both. The corresponding figures show that increasing the suction velocity reduces both the depth of the rotational layer and the magnitude of the velocity overshoot. Their behavior may be viewed as consistent with the results associated with an injection-driven oscillatory wave where the rotational layer thickens and its overshoot diminishes at higher injection velocities.[43,44] Increasing injection is clearly tantamount to decreasing wall suction.

V. Conclusions and Future Work

In this article, approximate solutions are obtained for the equations of motion describing the axisymmetric, viscous, laminar flow of a gas oscillating inside a porous tube with arbitrary levels of wall suction. In the process, the viscous Navier-Stokes equations are first linearized by separating the flow into a steady part and an oscillatory wave that is comparatively small. The unsteady flowfield is further partitioned based on the Helmholtz decomposition of the velocity vector. This decomposition leads to two sets of equations: the first describing a compressible, irrotational part, and the second alluding to an incompressible, rotational part. The compressible set is found to be equivalent to the organ pipe wave equation that is already known for the problem at hand. The solution of the rotational set then takes central stage in the remainder of this effort.

To proceed, the rotational momentum equation is split using separation of variables. This results in a second order ODE, referred to as the separated momentum equation, which must be solved to achieve closure. The separated momentum equation is found to be a doubly-perturbed problem whose solution requires the establishment of an asymptotic relation between the two large parameters in the problem, R and S. This asymptotic relation sets the trajectory of the asymptotic treatment of the separated momentum equation which is then pursued using both multiple-scales and WKB techniques.

Our findings indicate that the time-dependent flowfield remains intimately coupled to the mean flow and the latter can be represented by Berman's characteristic function $F(r)$. The ensuing wave approximations, which are developed though the application of multiple-scales and WKB techniques, are formulated in terms of an arbitrary mean flow function $F(r)$. Given the variety of mean flow solutions available in the literature, we find that a suitable profile for a particular motion is generally connected to the level of wall suction that it bears. The asymptotic solutions that we obtain can be applied to oscillatory flows with arbitrary levels of suction by simply inserting into our expressions the appropriate mean flow function. To illustrate the solution behavior, both multiple-scales and WKB approximations are compared to an exact solution that arises in the case of infinitely large suction. Based on this test case, we are able to ascertain that both of the perturbation solutions closely approximate the exact solution over a wide range of oscillation frequencies and wall suction velocities. The resulting approximations aid in understanding the multiple-scale structure of suction-driven oscillatory motions and increase our repertoire of engineering approximations for periodic flows.

Finally, in closing we note that both the multiple-scales and WKB solutions presented here become suddenly unbounded as $r \to 0$. In situations where highly accurate solutions are required in the core, the singularity at the core can be removed by adding endpoint correction terms to the solutions. The core singularity was also identified and corrected for in solutions of the injection driven planar flow in porous by Majdalani.[44] In future work, we plan to use a procedure similar to Majdalani's to determine the endpoint corrections to the solutions presented here, thus leading to the removal of the core singularity and the derivation of uniformly valid solutions.

Acknowledgments

This work was completed with the support received from the National Science Foundation through Grant No. CMMI-0928762.

References

[1]Berman, A. S., "Laminar Flow in Channels with Porous Walls," *Journal of Applied Physics,* Vol. 24, No. 9, 1953, pp. 1232-1235. doi: 10.1063/1.1721476

[2]Berman, A. S., "Effects of Porous Boundaries on the Flow of Fluids in Systems with Various Geometries," *Proceedings of the Second United Nations International Conference on the Peaceful Uses of Atomic Energy,* Vol. 4, 1958, pp. 351-358.

[3]Hartnell, J. P., and Eckert, E. R. G., "Mass-Transfer Cooling in a Laminar Boundary Layer with Constant Fluid Properties," *Transactions of the American Society of Mechanical Engineers,* Vol. 79, 1957, pp. 247-254.

[4]Vermeulen, P. J., Grabinski, P., and Ramesh, V., "Mixing of an Acoustically Excited Air Jet with a Confined Hot Crossflow," *Journal of Engineering for Gas Turbines and Power-Transactions of the ASME,* Vol. 114, No. 1, 1992, pp. 46-54. doi: 10.1115/1.2906306

[5]Vermeulen, P. J., Chin, C.-F., and Yu, W. K., "Mixing of an Acoustically Pulsed Air Jet with a Confined Crossflow," *Journal of Propulsion and Power,* Vol. 6, No. 6, 1990, pp. 777-783. doi: 10.2514/3.23284

[6]Rizzetta, D. P., "Numerical Simulation of Slot Injection into a Turbulent Supersonic Stream," *AIAA Journal,* Vol. 30, No. 10, 1992, pp. 2434-2439. doi: 10.2514/3.11244

[7]Rizzetta, D. P., and Visbal, M. R., "Large-Eddy Simulation of Supersonic Cavity Flowfields Including Flow Control," AIAA Paper 2002-2853, June 2002.

[8]Suzuki, N., Kiya, M., Mochizuki, O., and Jinzu, H., "Pulsating Round Jet in Cross Flow (Towards the Development of Flow Separation Control Device)," *Transactions of the Japan Society of Mechanical Engineers, Part B (Nippon Kikai Gakkai Ronbunshu, B Hen),* Vol. 63, No. 605, 1997, pp. 106-111.

[9]Ekaterinaris, J. A., "Numerical Investigations of Dynamic Stall Active Control for Incompressible and Compressible Flows," *Journal of Aircraft,* Vol. 39, No. 1, 2002, pp. 71-78. doi: 10.2514/2.2897

[10]Majdalani, J., and Van Moorhem, W. K., "Laminar Cold-Flow Model for the Internal Gas Dynamics of a Slab Rocket Motor," *Journal of Aerospace Science and Technology,* Vol. 5, No. 3, 2001, pp. 193-207. doi: 10.1016/S1270-9638(01)01095-1

[11]Majdalani, J., and Roh, T. S., "The Oscillatory Channel Flow with Large Wall Injection," *Proceedings of the Royal Society of London, Series A,* Vol. 456, No. 1999, 2000, pp. 1625-1657. doi: 10.1098/rspa.2000.0579

[12]Majdalani, J., and Zhou, C., "Moderate-to-Large Injection and Suction Driven Channel Flows with Expanding or Contracting Walls," *Journal of Applied Mathematics and Mechanics,* Vol. 83, No. 3, 2003, pp. 181-196. doi: 10.1002/zamm.200310018

[13]Majdalani, J., "The Oscillatory Channel Flow with Arbitrary Wall Injection," *Journal of Applied Mathematics and Physics (ZAMP),* Vol. 52, No. 1, 2001, pp. 33-61. doi: 10.1007/PL00001539

[14]Majdalani, J., "A Hybrid Multiple Scale Procedure for Boundary Layers Involving Several Dissimilar Scales," *Journal of Applied Mathematics and Physics (ZAMP),* Vol. 49, No. 6, 1998, pp. 849-868. doi: 10.1007/s000330050126

[15]Majdalani, J., and Rienstra, S. W., "Two Asymptotic Forms of the Rotational Solution for Wave Propagation inside Viscous Channels with Transpiring Walls," *Quarterly Journal of Mechanics and Applied Mathematics,* Vol. 55, No. 1, 2002, pp. 141-162. doi: 10.1093/qjmam/55.1.141

[16]Majdalani, J., Vyas, A. B., and Flandro, G. A., "Higher Mean-Flow Approximation for a Solid Rocket Motor with Radially Regressing Walls," *AIAA Journal,* Vol. 40, No. 9, 2002, pp. 1780-1788. doi: 10.2514/1.40061

[17]Maicke, B. A., and Majdalani, J., "On the Compressible Hart-McClure Mean Flow Motion in Simulated Rocket Motors," AIAA Paper 2010-7077, July 2010.

[18]Saad, T., and Majdalani, J., "On the Lagrangian Optimization of Wall-Injected Flows: From the Hart–McClure Potential to the Taylor–Culick Rotational Motion," *Proceedings of the Royal Society of London, Series A,* Vol. 466, No. 2114, 2010, pp. 331-362. doi: 10.1098/rspa.2009.0326

[19]Taylor, G. I., "Fluid Flow in Regions Bounded by Porous Surfaces," *Proceedings of the Royal Society of London, Series A,* Vol. 234, No. 1199, 1956, pp. 456-475. doi: 10.1098/rspa.1956.0050

[20]Maicke, B. A., and Majdalani, J., "On the Rotational Compressible Taylor Flow in Injection-Driven Porous Chambers," *Journal of Fluid Mechanics,* Vol. 603, No. 1, 2008, pp. 391-411. doi: 10.1017/S0022112008001122

[21]Saad, T., and Majdalani, J., "Rotational Flowfields in Porous Channels with Arbitrary Headwall Injection," *Journal of Propulsion and Power,* Vol. 25, No. 4, 2009, pp. 921-929. doi: 10.2514/1.41926

[22]Culick, F. E. C., "Rotational Axisymmetric Mean Flow and Damping of Acoustic Waves in a Solid Propellant Rocket," *AIAA Journal,* Vol. 4, No. 8, 1966, pp. 1462-1464. doi: 10.2514/3.3709

[23]Majdalani, J., and Saad, T., "The Taylor-Culick Profile with Arbitrary Headwall Injection," *Physics of Fluids,* Vol. 19, No. 9, 2007, pp. 093601-10. doi: 10.1063/1.2746003

[24]Majdalani, J., "On Steady Rotational High Speed Flows: The Compressible Taylor-Culick Profile," *Proceedings of the Royal Society of London, Series A,* Vol. 463, No. 2077, 2007, pp. 131-162. doi: 10.1098/rspa.2006.1755

[25]Srinivasacharya, D., Srinivasacharyulu, N., and Odelu, O., "Flow and Heat Transfer of Couple Stress Fluid in a Porous Channel with Expanding and Contracting Walls," *International Communications in Heat and Mass Transfer,* Vol. 36, No. 2, 2009, pp. 180-185. doi: 10.1016/j.icheatmasstransfer.2008.10.005

[26]Boutros, Y. Z., Abd-el-Malek, M. B., Badran, N. A., and Hassan, H. S., "Lie-Group Method Solution for Two-Dimensional Viscous Flow between Slowly Expanding or Contracting Walls with Weak Permeability," *Applied Mathematical Modelling,* Vol. 31, No. 6, 2007, pp. 1092-1108. doi: 10.1016/j.apm.2006.03.026

[27]Boutros, Y. Z., Abd-el-Malek, M. B., Badran, N. A., and Hassan, H. S., "Lie-Group Method for Unsteady Flows in a Semi-Infinite Expanding or Contracting Pipe with Injection or Suction through a Porous Wall," *Journal of Computational and Applied Mathematics,* Vol. 197, No. 2, 2006, pp. 465-494. doi: 10.1016/j.cam.2005.11.031

[28]Asghar, S., Mushtaq, M., and Hayat, T., "Flow in a Slowly Deforming Channel with Weak Permeability: An Analytical Approach," *Nonlinear Analysis: Real World Applications,* Vol. 11, No. 1, 2010, pp. 555-561. doi: 10.1016/j.nonrwa.2009.01.049

[29]Mahmood, M., Hossain, M. A., Asghar, S., and Hayat, T., "Application of Homotopy Perturbation Method to Deformable Channel with Wall Suction and Injection in a Porous Medium," *International Journal of Nonlinear Sciences and Numerical Simulation,* Vol. 9, No. 2, 2008, pp. 195-206.

[30]Dinarvand, S., and Rashidi, M. M., "A Reliable Treatment of a Homotopy Analysis Method for Two-Dimensional Viscous Flow in a Rectangular Domain Bounded by Two Moving Porous Walls," *Nonlinear Analysis: Real World Applications,* Vol. 11, No. 3, 2010, pp. 1502-1512. doi: 10.1016/j.nonrwa.2009.03.006

[31]Xu, H., Lin, Z. L., Liao, S. J., Wu, J. Z., and Majdalani, J., "Homotopy Based Solutions of the Navier-Stokes Equations for a Porous Channel with Orthogonally Moving Walls," *Physics of Fluids,* Vol. 22, No. 5, 2010, pp. 05360101-18. doi: 10.1063/1.3392770

[32]Yuan, S. W., "Further Investigation of Laminar Flow in Channels with Porous Walls," *Journal of Applied Physics,* Vol. 27, No. 3, 1956, pp. 267-269. doi: 10.1063/1.1722355

[33]Yuan, S. W., and Finkelstein, A. B., "Laminar Pipe Flow with Injection and Suction through a Porous Wall," *Transactions of the American Society of Mechanical Engineers: Journal of Applied Mechanics,* Vol. 78, No. 3, 1956, pp. 719-724.

[34]Sellars, J. R., "Laminar Flow in Channels with Porous Walls at High Suction Reynolds Numbers," *Journal of Applied Physics,* Vol. 26, No. 4, 1955, pp. 489-490. doi: 10.1063/1.1722024

[35]Terrill, R. M., and Thomas, P. W., "On Laminar Flow through a Uniformly Porous Pipe," *Applied Scientific Research,* Vol. 21, No. 1, 1969, pp. 37-67. doi: 10.1007/BF00411596

[36]Jankowski, T. A., and Majdalani, J., "Symmetric Solutions for the Oscillatory Channel Flow with Arbitrary Suction," *Journal of Sound and Vibration,* Vol. 294, No. 4-5, 2006, pp. 880-893. doi: 10.1016/j.jsv.2005.12.035

[37]Jankowski, T. A., and Majdalani, J., "Vortical and Acoustical Mode Coupling inside a Porous Tube with Uniform Wall Suction," *Journal of the Acoustical Society of America,* Vol. 117, No. 6, 2005, pp. 3448-3458. doi: 10.1121/1.1905639

[38]Jankowski, T. A., and Majdalani, J., "Laminar Flow in a Porous Channel with Large Wall Suction and a Weakly Oscillatory Pressure," *Physics of Fluids,* Vol. 14, No. 3, 2002, pp. 1101-1110. doi: 10.1063/1.1445419

[39]Majdalani, J., Zhou, C., and Dawson, C. A., "Two-Dimensional Viscous Flow between Slowly Expanding or Contracting Walls with Weak Permeability," *Journal of Biomechanics,* Vol. 35, No. 10, 2002, pp. 1399-1403. doi: 10.1016/S0021-9290(02)00186-0

[40]Richardson, E. G., and Tyler, E., "The Transverse Velocity Gradient near the Mouths of Pipes in Which an Alternating or Continuous Flow of Air Is Established," *Proceedings of the Physical Society,* Vol. 42, No. 1, 1929, pp. 1-15. doi: 10.1088/0959-5309/42/1/302

[41]Sexl, T., "Über Den Von E.G. Richardson Entdeckten 'Annulareffekt'," *Zeitschrift für Physik,* Vol. 61, No. 5-6, 1930, pp. 349-362. doi: 10.1007/BF01340631

[42]Uchida, S., "The Pulsating Viscous Flow Superposed on the Steady Laminar Motion of Incompressible Fluid in a Circular Pipe," *Journal of Applied Mathematics and Physics (ZAMP),* Vol. 7, 1956, pp. 403-422. doi: 10.1007/BF01606327

[43]Majdalani, J., and Flandro, G. A., "The Oscillatory Pipe Flow with Arbitrary Wall Injection," *Proceedings of the Royal Society of London, Series A,* Vol. 458, No. 2023, 2002, pp. 1621-1651. doi: 10.1098/rspa.2001.0930

[44]Majdalani, J., "Multiple Asymptotic Solutions for Axially Travelling Waves in Porous Channels," *Journal of Fluid Mechanics,* Vol. 636, No. 1, 2009, pp. 59-89. doi: 10.1017/S0022112009007939

[45]Majdalani, J., and Van Moorhem, W. K., "Improved Time-Dependent Flowfield Solution for Solid Rocket Motors," *AIAA Journal,* Vol. 36, No. 2, 1998, pp. 241-248. doi: 10.2514/2.7507

[46]Rott, N., "Theory of Time-Dependent Laminar Flows," *High Speed Aerodynamics and Jet Propulsion –Theory of Laminar Flows,* Vol. IV, edited by F. K. Moore, Princeton University Press, Princeton, New Jersey, 1964, pp. 395-438.

[47]Schlichting, H., *Boundary-Layer Theory*, 7th ed., McGraw-Hill, New York, 1979.